Tribological behavior of Ti(C, N)-TiB2 composite cermets using FeCoCrNiAl high entropy alloys as binder over a wide range of temperatures

Zhanjiang Li
Fujian University of Technology
Peixin Fu
Fujian University of Technology
Chenglong Zhu
Fuzhou University
Chunfu Hong
Fujian University of Technology
Pinqiang Dai (pqdai@126.com)
Fujian University of Technology

Research Article

Keywords: FeCoCrNiAl high-entropy alloys, Ti(C, N)-TiB2-HEAs composite cermets, High-temperature tribological properties, Wear mechanism

Posted Date: July 22nd, 2020

DOI: https://doi.org/10.21203/rs.3.rs-44863/v1

Version of Record: A version of this preprint was published at Materials Today Communications on March 1st, 2021. See the published version at https://doi.org/10.1016/j.mtcomm.2021.102095.

Abstract

The Ti(C, N)-TiB_2 composite cermets with different binders (HEAs or Ni-Co) were fabricated by mechanical alloying and vacuum hot-pressing sintering. Wear resistance of two composite cermets at elevated temperatures was studied. Wear mechanism was characterized by a combination of scanning electron microscopy and energy dispersive spectroscopy. Experimental results indicated that HEAs binder composite cermets possessed excellent wear resistance comparing with Ni-Co binder composite cermets. At lower temperatures, no obvious difference was observed in worn surfaces of two cermets. Abrasive wear mechanism was dominant wear mechanism. At greater than 600 °C, oxidative wear and adhesive wear were found to be dominant wear mechanism. The wear rate of HEAs binder composite cermets was 11.8%, 17%, 39.25%, and 46.7% lower than that of Ni-Co binder composite cermets at 200℃, 400℃, 600℃, and 800℃, respectively. Enhanced wear performance of Ti(C, N)-TiB_2-HEAs composite cermets is attributed to relatively high hardness and toughness, as well as excellent high-temperature softening resistance and oxidation resistance of HEAs.

1 Introduction

WC-Co cemented carbide is widely used in machining, metallurgy, aerospace and other fields, attributing to its high hardness, strength, wear resistance, and corrosion resistance [1–4]. However, with decreasing global tungsten resources and the increase in cobalt price in recent years, alternative materials for cemented carbide are desperately needed for some aspects. After years of development, Ti(C, N)-based cermet materials have received extensive attention attributing to their high hardness, excellent wear resistance, thermal shock resistance, and high-temperature oxidation resistance. Cemented carbides have been successfully replaced in terms of finishing and semi-finishing as cutting tools [5, 6].

Usually, the cutting temperature of cermet cutting tools can reach in the range 600–1000 °C, and this working condition is quite severe during the dry finishing and semi-finishing process [7]. Under this situation, cermet tools with excellent thermomechanical properties, thermal shock resistance, and high-temperature resistance friction and softening resistance are required. Therefore, as a high-temperature material, they must have excellent resistance to high temperature. High-temperature anti-wear properties have become more important than other mechanical properties such as toughness and mechanical shock resistance indicators for evaluating tool materials [8–10]. In recent years, the friction and wear properties of Ti(C, N) based cermets have been studied by many researchers [11–14]. Verma *et al.* [11] found the coefficient of friction (COF) of Ti(C, N)-based cermets with or without TaC as 0.3 to 1.1. Stewart *et al.* [12] reported that the addition of Mo_2C had a detrimental effect on the sliding wear response of the Ti(C, N) based cermets. Yang *et al.* [13, 14] investigated the high-temperature friction and wear properties of TiN–TiB_2 ceramic and found that lubricious oxidized products had a favorable effect on ceramic at high temperature. However, these studies mainly focused on the addition phase, and the effect of the binder phase of Ti(C, N)-based cermets on the friction and wear properties at high temperature has been scarcely investigated. In addition, the Fe, Co, and Ni traditional binders have high-temperature softening

and poor oxidation resistance characteristics. Consequently, exploring new binders is important. High entropy alloy (HEA) is a new type of multi-component alloy with many excellent properties such as high strength, hardness, wear resistance and thermal stability [15–16]. It has been used to replace traditional adhesives to improve the high-temperature performance of cermets, which has gradually attracted researchers' attention, resulting in some outstanding findings. [17–21]. However, the effect of HEAs binder on the wear properties of Ti(C, N) based cermets at high temperature is still unclear. FeCoCrNiAl HEAs possess excellent high-temperature performance [18, 22]. Therefore, in this study, the FeCoCrNiAl HEAs were selected as the binder compared to the traditional Ni-Co binder.

The focus of this study was to research the high-temperature friction and wear behavior of Ti(C, N)- TiB_2 composite cermets with HEAs or Ni-Co as the binder. The COF and specific wear rate were investigated, and wear mechanisms were analyzed. This study will provide a useful reference for the selection of cermet binders in the future.

2 Experimental

The cermet in this experiment was prepared by the powder metallurgy method. The compositions (wt.%) of the Ti(C, N)-based cermet in this study were Ti(C, N)-TiB_2-(10 wt.%) HEAs or (10 wt.%) Ni-Co. The Ti(C, N) and TiB_2 mass ratio was 3:1. Commercially available Fe, Co, Cr, Ni, Al, Ti(C, N) and TiB_2 were supplied by Shuitian Technology Co., Ltd., Shanghai, China. Associated purities and particle sizes are shown in Table 1. The FeCoCrNiAl HEAs powder was prepared by mechanical alloying (MA) method using a QM-QX full planetary ball mill (Mickey Technology Co., Ltd., Changsha, China). The ball ratio, ball mill, and rotating speed were 15:1, 30 h, and 250 r/min, respectively.

Powder mixtures of Ti(C, N)-TiB_2-FeCoCrNiAl HEAs (denoted as CBH) and Ti(C, N)-TiB_2-Ni-Co (denoted as CBN) were obtained using a wet ball-miller in a stainless steel ball mill tank with stainless steel ball and ethyl alcohol as the media for 24 h at a rotation speed of 150 r/min with a ball-to-powder mass ratio of 10:1. The mixed powder was poured into a stainless steel dish and placed in a DZF-6050 vacuum drying oven, and dried at 70 °C for 15 h, and then, passed through a 100 mesh screen. A vacuum hot-pressing sintering furnace (ZT-40-21Y, Shanghai, China) was used to sinter cylindrical blocks with a diameter of 30 mm and a height of 7 mm. The sintering temperature, hold temperature time, and hold temperature pressure were 1500 °C, 30 min, and 34 MPa, respectively. The samples were cooled in the furnace.

The Archimedes principle is used to measure the bulk density of sintered samples. The Vickers hardness tester (model HVST-10, China) was used to test the hardness under a load of 98 N. The three-point bending method was adopted to test the bending strength through an electronic universal tester (China WD-10). The indentation method was used to test

fracture toughness and was calculated using Palmqvist-type cracks around the indentation according to the Niihara formula represented by Eq. (1) [23]:

$$K_{IC} = 0.035(Ha^{1/2})(E\emptyset/H)^{0.4}\,(l/a)^{-1/2}/\emptyset \quad (1)$$

Where H is the Vickers hardness, E is the elastic modulus (480 GPa), a is the indentation half length, l is the crack length, and Φ is the shape factor (= 3).

The friction and wear were tested using a high-temperature vacuum friction and wear testing machine (Model HVT-1000 Lanzhou, China). With regard to counter body material, the choice of cemented carbide (WC-6Co) with Ø4 mm (Linwei Steel Ball Co., Ltd., Hangzhou, China) was mainly attributed to the cemented carbide regularly used in all crushing & grinding operations and partially was replaced by Ti(C, N) based cermets in cutting tool. Under these circumstances, cemented carbide as a counter-grinding material can have a significant contrast with the research material. And the components and properties of WC-6Co ball are listed in Table 2. Specimens with Ø30×2 mm^3 dimensions were cut from the as-sintered cylindrical bars, ground, polished, and dried. The test sliding velocity, load, and sliding time were 450 rpm, 5 N, and 20 min, respectively. The tests were carried out at 200, 400, 600, and 800 °C. Wear rates were calculated by Eq. (2).

$$W_r = \frac{V_r}{S \times F} \quad (2)$$

where Wr is the volume wear rate (mm^3/Nm), V_r is the volume loss of the material, S is the sliding distance, and F is the applied normal force. S is given by $S = v \times r \times t$, where v, r, and t are the rotational speed, track diameter, and time, respectively.

High temperature vacuum hardness tester (Model HVT-1000 Lanzhou, China) is used to test the thermal hardness of cermets under a load of 196 N. SEM was used to measure the diagonal length of the indentation. Then, the average of the two diagonal lines was calculated and the appropriate hardness was compared with the Vickers hardness standard table. The final hardness is taken from the average of five points.

The phase constituents of these wear surfaces were analyzed by X-ray diffraction (XRD) (D8 Advance, Germany). The microstructure of the specimens and wear scar was observed by scanning electron microscopy (SEM) (FEI NovaNanoSEM450, America). The chemical composition was analyzed by energy dispersive spectrometry (EDS) (Model Link-ISIS, Oxford, England). The chemical compounds on the wear surface were determined by X-ray photoelectron spectroscopy (XPS).

3. Results

3.1 Microstructure and mechanical properties

The microstructures and fracture morphology of the sintered CBH and CBN composite cermets are shown in Fig. 1. Based on previous study [24], in Fig. 1(a) and (b), the gray matrix and dark gray massive particles are Ti (C, N) and TiB_2. The white phase distributed between TiB_2 and Ti(C, N) is HEAs (Fig. 1(a)) or Ni-Co (Fig. 1(b)). In Fig. 1(a), the black phase is Al_2O_3 or pores. The CBH composite cermets (Fig. 1(c)) mainly exhibited transgranular fracture mode, which could consume more energy to improve their toughness. However, the CBN composite cermets (Fig. 1(d)) mainly have intergranular fracture, indicating that the binder and ceramic phase bind poorly. The density and mechanical properties are listed in Table 3. Clearly, the CBH composite cermets have a density of 4.992 g/cm^3 and exhibit relatively excellent mechanical properties with a Vickers hardness of 1977.3 HV_{10}, fracture toughness of 7.9 MPa $m^{1/2}$, and a bending strength of 727 MPa at room temperature.

3.2 Friction and wear characteristics

Fig. 2 depicts the COF of two cermet composites at different temperatures, clearly indicating that the COF values of the two composite materials have the same tendency with temperature. At the beginning of the experiment, the friction coefficient gradually increases and then reaches a steady state. In general, this process can be divided into two stages: wearing-in stage and stable wear, which are similar to the literature [25]. At the beginning, the interface is very rough, and the contact area at the micro protrusions is small, so it will be worn away, which will cause the contact point to have a cold welding effect. High shear forces are required to cut the welds, which will rapidly increase the coefficient of friction at the beginning of the running-in phase [25]. With increasing friction time, the friction coefficient became relatively stable and is mainly attributed to the contact area achieving running-in stage, and the relatively rough contact surface is replaced by a relatively smooth friction layer. With increasing testing temperature, the COF decreases first and then increases. The CBH and CBN had the highest COF of 0.36 and 0.41, respectively, at 200 °C (Fig. 3), and the minimum is 0.27 and 0.32, respectively, at 400 °C (Fig. 3). In addition, the COF increased to 0.29 and 0.37 at 600 °C for the CBH and CBN, respectively (Fig. 3), attributed to the high temperature, which softens the sample and grinding ball and forms a soft oxide layer on the sample surface, resulting in slight adhesive wear. The COF reached 0.23 and 0.35 at 800 °C (Fig. 3). This might be due to tribo-oxidation wear and adhesive wear. Relatively low COF values were obtained compared to the literature data [13]. The difference in the friction coefficient indicates that the binder (HEAs and Ni-Co) has an

important effect on the COF of the material. The mechanism of the effect of the binder is discussed in detail below.

Fig. 4 shows the effect of temperature and wear rate of two cermet composites, indicating that CBH has a lower wear rate than CBN at different test temperatures. With increasing test temperature, the wear rate increases first and then decreases. The relatively higher wear rate of the CBN is mainly because of the low strength of the Ni-Co binder, easily producing the wear debris. CBH composites have a relatively low wear rate, which might be the effect of HEAs binders. FeCoCrNiAl HEAs have excellent high-temperature softening resistance [26], endowing the CBH composites with excellent mechanical properties at high temperature. Table 3 shows that the CBH composites exhibited better hardness, strength, and toughness than those of the CBN composites. In general, the wear is related to the hardness and plastic deformation of materials. Eq. (3) shows that the wear volume of the material is inversely proportional to the hardness and toughness, explaining the CBH composites having a lower wear rate than that of the CBN composites [27,28].

$$V = \alpha \frac{P^{9/8}}{K_C^{1/2} H^{5/8}} (E/H)^{4/5} \quad (3)$$

where V is the volume wear rate, α is the material-independent constant, K_C is the toughness, P is the normal load, E is the Young's modulus of materials, and H is the hardness. The test temperature plays an important role in evolution of friction and wear of materials. With increasing test temperature to 600 °C, the wear rate of the two materials reduced dramatically, and this might be relative to the change in the wear mechanism and the decreased hardness of the coupled grinding ball.

3.3 Wear surface morphology

Fig. 5 shows the wear surface morphology of the CBH and CBN composites at different temperatures, indicating that the testing temperature has a significant effect on the wear scar morphology of the composite, especially at >600 °C. The difference in the wear surface is not obvious at 200 °C and 400 °C, all of which are formed by the repeated action of abrasive wear, forming of a large number of shallow grooved scratches and hard particle debris of compaction. The wear mechanism is mainly abrasive wear. With increasing test temperature, the worn surface of the two materials changed obviously. This may be the effect of different binders. For the CBH composites, at 600 °C, there are two different wear scar morphologies in the middle and boundary of the wear scar. In the middle is a dense plow, which is characteristic of the abrasive wear. At the boundary, scattered wear debris and a small amount of adhesive were observed. This may be attributed to the softening of the binder and the grinding ball or the relatively soft and highly adherent oxides (TiO_2, WO_3, etc.), mutually transferring the tribo-layers. At 600 °C,

the wear surface of the CBN composite did not show any adhesive, but large ploughs and debris appeared. This may be because the abrasive wear was produced between the larger convex hard particles on the grinding ball and the softer surface of the sample surface [29]. As the test temperature rises to 800 °C, the wear scar surface of the CBH composite has a relatively shallow and flat plow marks (Fig. 5(d)). At high temperature, the surface of the sample and the grinding ball oxidized in the oxygen environment. During the wear process, some relatively soft and highly adherent oxides (TiO_2, WO_3, etc) are repeatedly extruded, stretched, and finally spread on the wear surface of the sample to form a dense friction layer. Moreover, HEAs also have excellent oxidation resistance [30,31]. The above features will effectively prevent the infiltration of oxygen and the further oxidation of the substrate, thus may reduce the wear rate of CBH composites. However, the wear surface of the CBN composite still exhibits ploughs and debris of abrasive wear at 800 °C (Fig. 5(f)) despite a dense tribo-layer of particles. The CBN composite has a relatively poor density, more easily infiltrating oxygen, resulting in a thicker oxide layer. In addition, the relatively low strength and toughness make the grains easier to pull out during high-temperature wear, leading to a poor wear performance of the CBN composite.

4 Discussion

Wear mechanism at high temperature (600 and 800 °C)

Based on the above analysis of the wear surface morphology, the wear mechanism of the material at 600 and 800 °C is discussed in detail below. In general, the wear mechanisms of cermet materials are typically brittle fracture, grain extraction, and tribo-oxidation wear, as determined by mechanical wear [32, 33]. However, with increasing testing temperature, the proportion of tribo-oxidation wear will greatly increase because of the oxygen environment. Figure 7 shows the high magnification images of the wear morphology and the grinding ball wear morphology of both composites at 600 and 800 °C. Obviously, a small amount of pits and debris are observed on the surface of the CBH composite, most of which is compacted at 600 °C (Fig. 6(a)). However, the surface of the CBN composite was covered with a large amount of small debris. The EDS analysis (regions 1 and 5 in Figs. 6(a) and (e) Table 4) showed the presence of oxygen, indicating that tribo-oxidation wear also occurred during the wear process.
Figure 6(b) shows the wear morphology of the CBH composite grinding ball at 600 °C. A small amount of adhesive was observed on the edge of the grinding ball wear scar. The combined analysis results of Fig. 5(c) and EDS analysis (regions 2 and 6 in Figs. 6(b) and (f) Table 4) indicate that the adhesive is mainly a friction layer, which is transferred from the substrate. However, the surface of the grinding ball of Fig. 6(f) has more adhesives than that observed in Fig. 6(b). These characteristics indicated that the CBN composite has strong adhesive wear at 600 °C, attributed to relatively higher high-temperature hardness of CBH than CBN and excellent high-temperature softening resistance of HEA (Fig. 7). In general, hardness is related to the dislocation slip system in the material [34]. Under high temperature conditions, dislocations are first formed in the binder, and then the dislocations enter the hard phase. Finally, the

overall plastic deformation occurs in the stressed area of the cermet [35]. The HEAs binder is prone to form twins relative to the elemental metal binder, because of its low stacking fault energy. Under these conditions, the twins will hinder the movement of dislocations, improving the hardness of ceramic materials [36]. When the material shows a slight adhesive wear, the adhesion of the friction pair contact area is lower than the shear strength of the two materials. At this time, the friction coefficient increases, the wear rate decreases, and the material transfer is not obvious. This is consistent with the adhesive wear of the CBH composites at 600 °C. However, when the adhesive wear becomes strong, the adhesion of the friction pair contact area is higher than the shear strength of the softer material in the friction pair. The damage occurs in the surface layer of the softer material near the contact surface; therefore, the soft material is transferred to the surface of the hard material. At this time, the friction coefficient is similar to slight adhesive wear, but the relative wear rate is aggravated. This is consistent with the adhesive wear of the CBN composites at 600 °C.

The CBH composite has a relatively smooth wear surface at 800 °C (Fig. 6(c)) versus 600 °C (Fig. 6(b)). The EDS analysis (regions 3 in Fig. 6(c) and Table 4) shows that the wear surface forms a dense oxide layer. In this case, the tribo-oxidation wear is the main wear mechanism. In addition, the lowest wear rate of the CBH composites indicates that the dense oxide layer has a beneficial effect on the wear properties of the material. At high temperatures, both the ball and the material soften, and the surface is oxidized. In this case, the friction mainly occurs between the softening layer and the oxide layer. The plastic deformation of the friction layer results in the formation of a dense friction surface at the friction interface, and the FeCoCrNiAl HEAs have excellent high-temperature oxidation resistance [18], which can prevent further oxidation of the matrix and effectively reduces the wear. Regarding the CBN composite, the friction surface is relatively rough. The EDS analysis (regions 7 and 8 in Figs. 6(g) and (h) Table 4) shows that the substrate and grinding ball wear surface have mutual transfer of elements. In addition, not only the plow marks, but also the extraction of grains is observed. These features demonstrate that the CBN composite exhibited tribo-oxidation wear, adhesive wear, and abrasive wear at 800 °C, mainly because of their low hardness at 800 °C, causing strong wear. Figure 8 shows the depth of the wear of the two materials at 800 °C, with CBN composite exhibiting deeper wear than that of the CBH composite.

To further confirm the high-temperature wear mechanism, Ti and W elements on the worn surfaces of CBH and CBN composite cermets at 600 and 800 °C were analyzed by XPS, as shown in Fig. 9. For the CBH composite cermets, as shown in Figs. 9(a) and (c), the main peak of Ti2p of the worn surface appears at 458.4 ± 0.1 eV, which are assigned to the TiO_2 [37]. The analysis of W elements shows that the peaks also include WC besides tungsten oxide [38]. However, the peaks of CBN composite cermets did not show any obvious change. The results indicated that the worn surface mainly composed of oxides of Ti and W. In addition, the presence of the WC peak further demonstrates the occurrence of adhesive wear of the CBH composite cermets at 600 and 800 °C.

5 Conclusions

The wear resistance of Ti(C, N)-TiB_2 composite cermets for different binders (HEAs and Ni/Co) at high-temperature against WC-6Co was studied. The conclusions of this study are summarized as:

1. The Ti(C, N)-TiB_2 composite cermets with HEAs binder had better wear resistance than that of the composite with traditional Ni/Co binder. And as the test temperature increases, the abrasion resistance of CBH composite cermets increases. For example, the wear rate of CBH composite cermets was 11.8%, 17%, 39.25%, and 46.7% lower than that of CBN composite cermets at 200℃, 400℃, 600℃, and 800℃, respectively.
2. The wear mechanisms of the composite cermets are affected by the binder and test temperature. At 200 °C and 400 °C, the abrasive wear plays important roles. The abrasive wear and tribo-oxidation wear are the dominant wear mechanisms of the composite cermets, and mild adhesive wear was observed at 600 °C.
3. At 800 °C, the dense oxide layer of the wear surface prevents further tribo-oxidation wear, provides excellent lubrication effect, and greatly decreases the COF of the CBH composite cermets. The tribo-oxidation wear is the dominant wear mechanism. However, the wear mechanisms of the CBN composite cermets also include slight abrasive wear besides tribo-oxidation wear.

Conflict Of Interest

The authors declare that they have no conflict of interest.

References

1. Liu X, Song X, Wang H et al (2018) Complexions in WC-Co cemented carbides. Acta Mater 149:164–178
2. Chang S, Chen S (2014) Characterization and properties of sintered WC–Co and WC –Ni–Fe hard metal alloys. J Alloys Compd 585:407–413
3. Materials H, García J, Ciprés VC et al (2019) Cemented carbide microstructures: a review. Int J Refract Met Hard Mater 80:40–68
4. Liu X, Zhang J, Hou C et al (2018) Mechanisms of WC plastic deformation in cemented carbide. Mater Des 150:154–164
5. Jeon ET, Joardar J, Kang S (2002) Microstructure and tribo-mechanical properties of ultrafine Ti(C,N) cermets. Int J Refract Met Hard Mater 20:207–211
6. Peng Y, Miao H, Peng Z (2013) Development of TiCN-based cermets: Mechanical properties and wear mechanism. Int J Refract Met Hard Mater 39:78–89
7. Zhao XZ, Liu JJ, Zhu BL et al (1997) Friction and Wear of Si_3N_4 Ceramic / Stainless Steel Sliding Contacts in Dry and Lubricated Conditions. J Mater Eng Perform 6:203–208
8. Abukhshim NA, Mativenga PT, Sheikh MA (2006) Heat generation and temperature prediction in metal cutting: A review and implications for high speed machining. Int J Machine Tools Manuf

46:782–800

9. Yashiro T, Ogawa T, Sasahara H (2013) International Journal of Machine Tools & Manufacture Temperature measurement of cutting tool and machined surface layer in milling of CFRP. Int J Mach Tools Manuf 70:63–69
10. Bellosi A (2001) Factors inuencing the milling performances of Ti(C,N)-based tools against carbon steel. Int J Refract Met Hard Mater 19:191–202
11. Verma V, Kumar BVM (2017) Sliding wear behavior of SPS processed TaC-containing Ti(C,N)-WC-Ni/Co cermets against Silicon Carbide. Wear 376–377:1570–1579
12. Ni TN, Stewart TL, Plucknett KP (2015) The effects of Mo_2C additions on the microstructure and sliding wear of $TiC_{0.3}N_{0.7}$–Ni_3Al cermets. Int J Refract Met Hard Mater 50:227–239
13. Yang Z, Ouyang J, Liu Z et al (2010) Wear mechanisms of TiN–TiB_2 ceramic in sliding against alumina from room temperature to 700 ℃. Ceram Int 36:2129–2135
14. Yang Z, Ouyang J, Liu Z et al (2013) Microstructure and tribological properties of reactive hot pressed TiN–TiB_2 composites incorporated with or without $MoSi_2$ from room temperature to 800 ℃. Wear 301:641–647
15. Zhang Y, Ting T, Tang Z et al (2014) Progress in Materials Science Microstructures and properties of high-entropy alloys. Prog Mater Sci 61:1–93
16. Yeh JW, Chen S, Lin S et al (2004) Nanostructured High-Entropy Alloys with Multiple Principal Elements: Novel Alloy Design Concepts and Outcomes. Adv Eng Mater 6:299–303
17. Ji W, Zhang J, Wang W et al (2014) Fabrication and properties of TiB_2-based composite cermets by spark plasma sintering with CoCrFeNiTiAl high-entropy alloy as sintering aid. J Eur Ceram Soc 35:879–886
18. Zhu G, Liu Y, Ye J (2014) Early high-temperature oxidation behavior of Ti(C,N) -based composite cermets with multi-component AlCoCrFeNi high-entropy alloy binder. Int J Refract Met Hard Mater 44:35–41
19. Chen C, Yang C, Chai H et al (2014) Novel cermet material of WC / multi-element alloy. Int J Refract Met Hard Mater 43:200–204
20. Zhou PL, Xiao DH, Zhou PF et al (2018) Microstructure, and properties of ultra fi ne grained AlCrFeCoNi/WC cemented carbides. Ceram Int 44:17160–17166
21. He Z, Wang M (2017) Novel cemented carbide produced with $TiN_{0.3}$ and high-entropy alloys. Rare Met 36:494–500
22. Joseph J, Haghdadi N, Shamlaye K et al (2019) The sliding wear behaviour of CoCrFeMnNi and AlxCoCrFeNi high entropy alloys at elevated temperatures. Wear 428–429:32–44
23. Niihara K (1983) A fracture mechanics analysis of indentation-induced Palmqvist crack in ceramics. J Mater Sci Lett 2:221–223
24. Li Z, Liu X, Guo K et al (2019) Microstructure and properties of Ti(C,N)–TiB_2–FeCoCrNiAl high-entropy alloys composite cermets. Mater Sci Eng A 767:138427

25. Fang Y, Chen N, Du G et al (2019) High-temperature oxidation resistance, mechanical and wear resistance properties of Ti(C,N)-based cermets with $Al_{0.3}$CoCrFeNi high-entropy alloy as a metal binder. J Alloys Compd 815:152486
26. Ji W, Fu Z, Wang W et al (2014) Mechanical alloying synthesis and spark plasma sintering consolidation of CoCrFeNiAl high-entropy alloy. J Alloys Compd 589:61–66
27. Evans AG, Marshall DB, Wear mechanisms in ceramics, Funda. Frict. *Wear Mater*. 1980, 439–452
28. Yang CT, Wei WJ (2000) Effects of material properties and testing parameters on wear properties of fine-grain zirconia (TZP). Wear 242:97–104
29. Harsha AP, Tewari US (2003) Two-body and three-body abrasive wear behaviour of polyaryletherketone composites. Polym Test 22:403–418
30. Butler TM, Weaver ML (2016) Oxidation behavior of arc melted AlCoCrFeNi multi-component high-entropy alloys. J Alloys Compd 674:229–244
31. Crfeconisi A, Chen L, Zhou Z et al (2018) High temperature oxidation behavior of $Al_{0.6}$CrFeCoNi and $Al_{0.6}CrFeCoNiSi_{0.3}$ high entropy alloys. J Alloys Compd 764:845–852
32. Skopp A, Woydt M, Tribological behavior of silicon nitride materials under unlubricated sliding between 22 ℃ and 1000 ℃, *Wear*. 1995, 183
33. Hsu SM, Shen M (2004) Wear prediction of ceramics. Wear 256:867–878
34. Alpert CP, Chan HM, Bennison SJ et al (1998) Temperature dependence of hardness of alumina-based ceramics. J Am Ceram Soc 71:371–373
35. Bolognini S, Feusier G, Mari D et al (2003) TiMoCN-based cermets: high-temperature deformation. Int J Refract Metals Hard Mater 21:19–29
36. Dunand D, Mortensen A (1991) Reinforced silver chloride as a model material for the study of dislocations in metal matrix composites. Mater Sci Eng A 144:179–188
37. Meng J, Lu J, Wang J et al (2006) Tribological behavior of TiCN-based cermets at elevated temperatures. Mater Sci Eng A 418:68–76
38. Chen L, Yi D, Wang B et al (2016) Mechanism of the early stages of oxidation of WC–Co cemented carbides. Corrosion Sci 103:75–87

Acknowledgements

This work was supported by University Industry-University Cooperation Project of Fujian Province [Grant Number 2014H6005 and 2019H6022].

Tables

Table 1 Purity and particle size of the used powders.

Table 2 Chemical composition, density and mechanical properties of counter body material of WC-Co.

Table 3 Relevant properties of the Ti(C, N)-TiB_2-FeCoCrNiAl HEAs/Ni-Co composite cermets.

Table 4 Results of EDS analysis for the worn surfaces of the sample and the WC/Co ball in Fig. 6.

Table 1

Powder	Fe	Co	Cr	Ni	Al	Ti(C,N)	TiB_2
Purity/wt.%	99.9	99.9	99.9	99.9	99.9	99.9	99.9
Particle size/μm	<5.0	<5.0	<5.0	<5.0	<5.0	<1.0	<1.0

Table 2

Material	Chemical composition (%)		Density (g/cm^3)	mechanical properties	
YG6 (WC-Co)	WC	Co	14.95	Hardness (HRA)	Bending strength (MPa)
	94	6		90.5	1850

Table 2

Sample	Density (g/cm^3)	Vickers hardness (HV_{10})	Fracture toughness (MPa $m^{1/2}$)	Bending strength (MPa)
CBH	4.992	1977.3 ±20	7.9 ± 0.1	727 ± 20
CBN	4.815	1905.4 ± 20	6.8 ± 0.1	615 ± 20

Table 3

Type of study		Location	Element [at. %]										
			Ti	C	N	B	O	W	Fe	Co	Cr	Ni	Al
EDS	Fig. 6(a)	1	41.4	25.7	8.9	-	24.6	4.4	1.5	-	-	-	0.9
	(b)	2	37.8	25.0	8.9	-	17.0	5.5	2.0	1.5	1.1	-	1.2
	(c)	3	19.2	16.3	5.3	-	52.9	2.7	1.1	1.4	0.5	-	0.7
	(d)	4	34.9	26.2	13.6	-	18.3	3.3	0.9	0.9	0.6	-	1.4
	(e)	5	47.6	15.3	-	-	35.2	1.2	-	0.7	-	-	-
	(f)	6	46.4	21.9	5.0	12.8	11.1	1.6	-	-	-	1.2	-
	(g)	7	35.1	18.0	-	-	45.8	1.1	-	-	-	-	-
	(h)	8	22.1	31.1	8.3	13.4	12.5	10.7	-	1.7	-	0.2	-

Figures

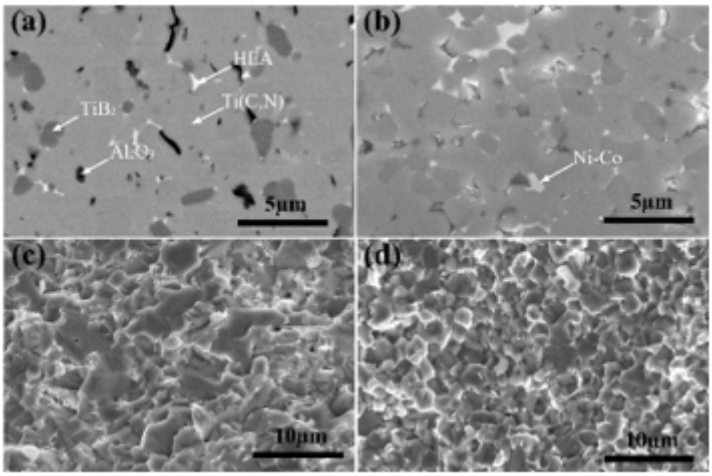

Figure 1

The microstructure and fracture morphology images of the sintered Ti(C, N)-TiB2- FeCoCrNiAl HEAs/Ni-Co composite cermets. (a) and (c): sample CBH; (b) and (d): sample CBN.

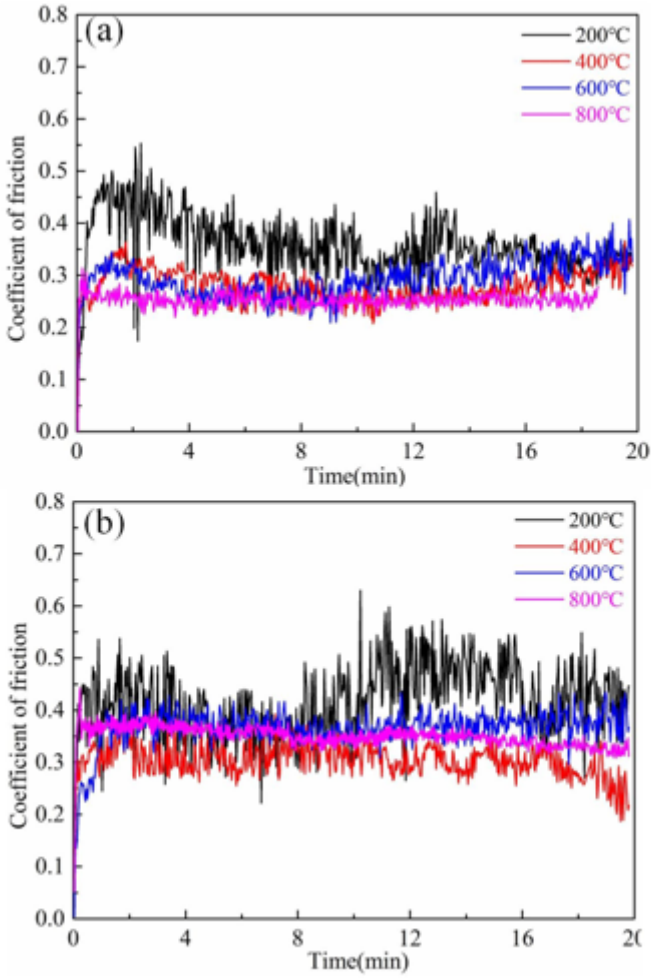

Figure 2

Dependency of friction coefficient with sliding time for CBH and CBN composite cermet against WC-Co ball at different temperatures: (a) CBH omposite cermet, (b) CBN omposite cermet.

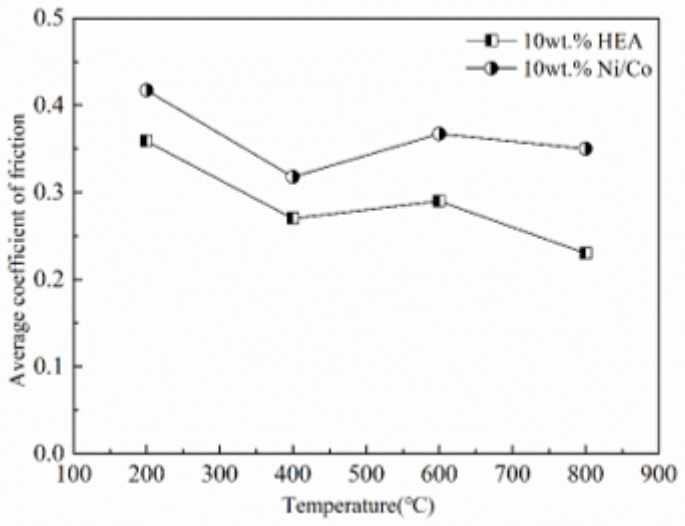

Figure 3

Influence of HEA binder and Ni/Co binder on wear coefficient of omposite cermet.

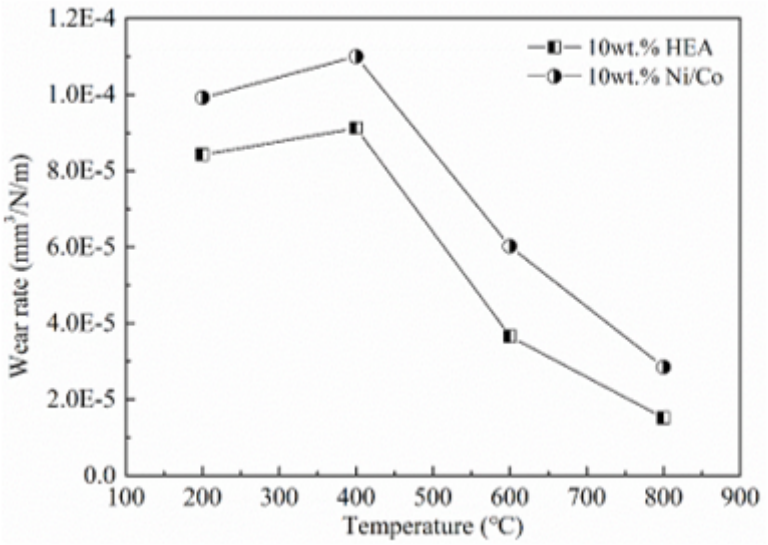

Figure 4

Influence of HEAs binder and Ni/Co binder on wear rate of omposite cermet.

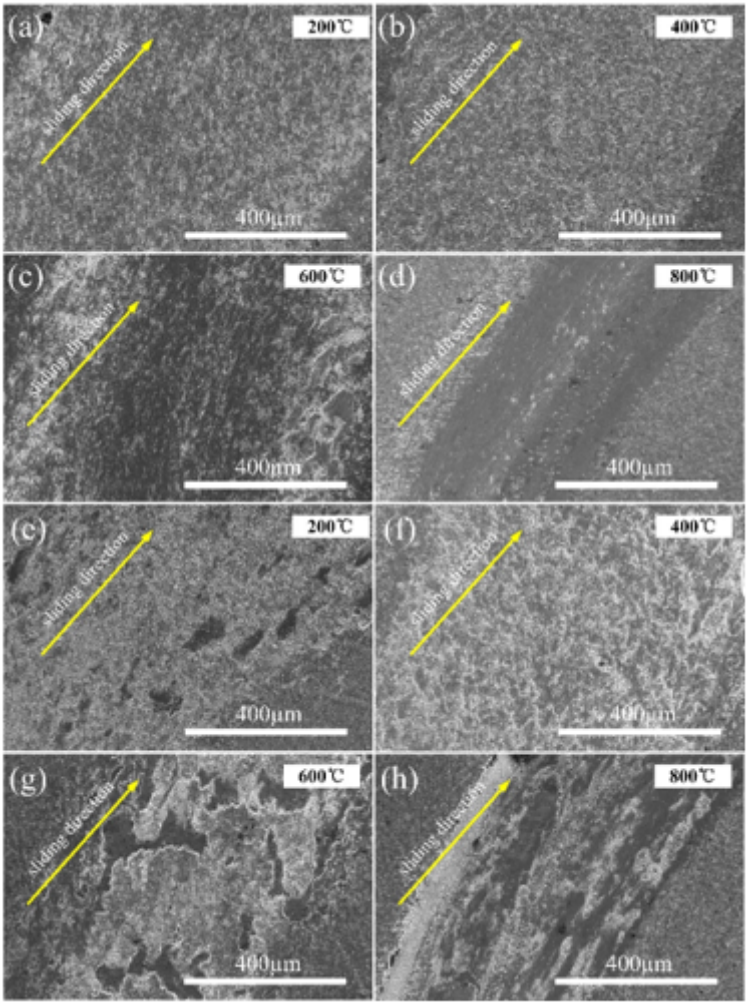

Figure 5

The wear scar morphology of CBH composites and CBN composites at different temperatures: (a), (b), (c), and (d) CBH composites; (e), (f), (g), and (h) CBN composites.

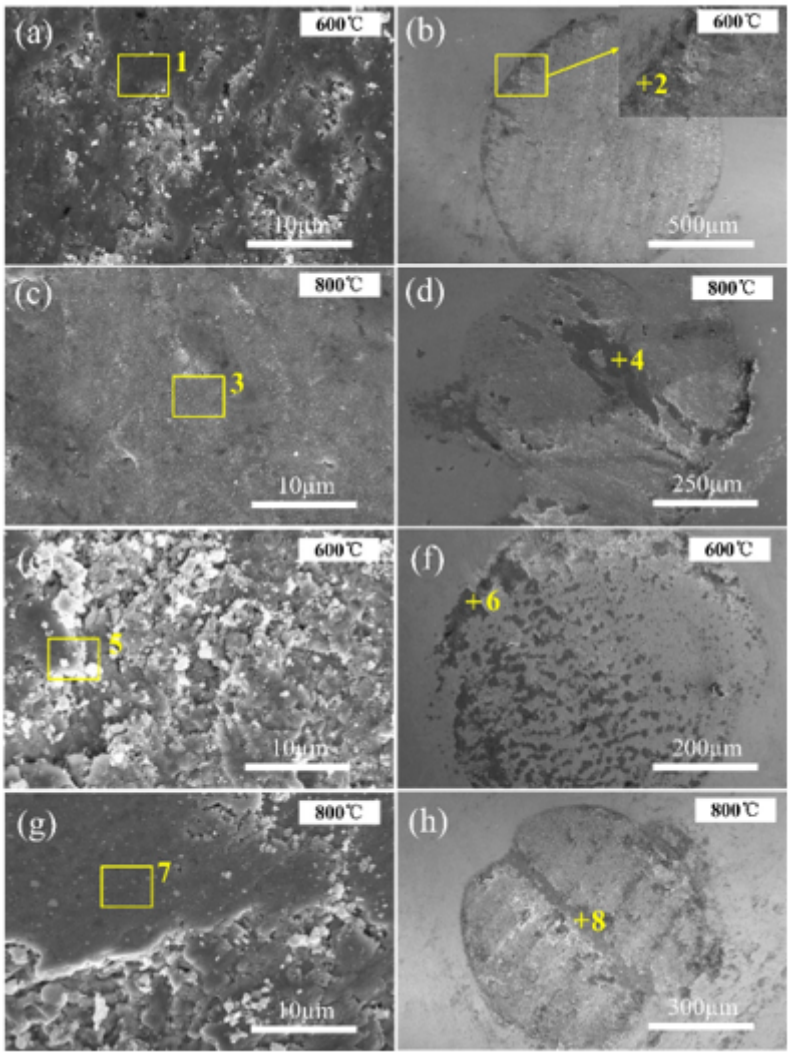

Figure 6

Worn surfaces of the sample and the WC/Co ball at 600 and 800 °C: (a) and (c) the CBH composites; (e) and (g) the CBN composites; (b), (d), (f), and (h) the WC/Co ball.

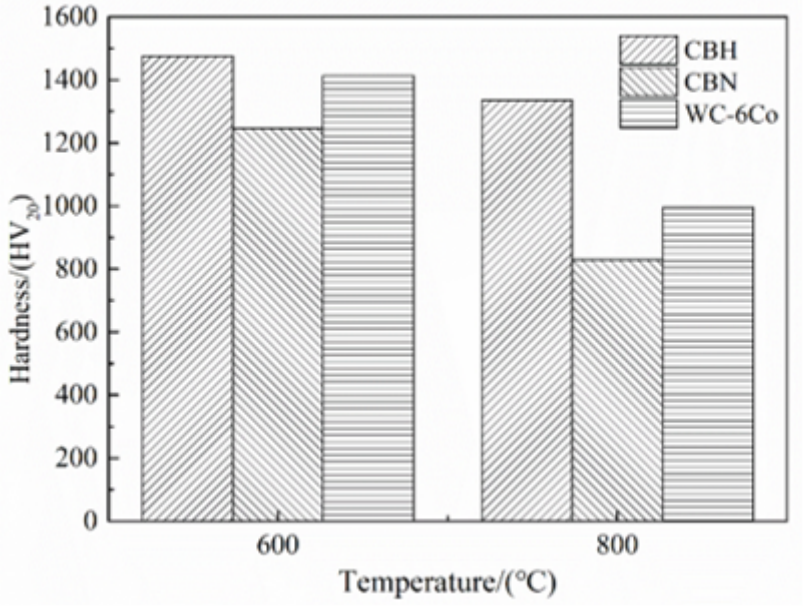

Figure 7

The high-temperature hardness of CBH, CBN and WC-6Co at 600 and 800 °C.

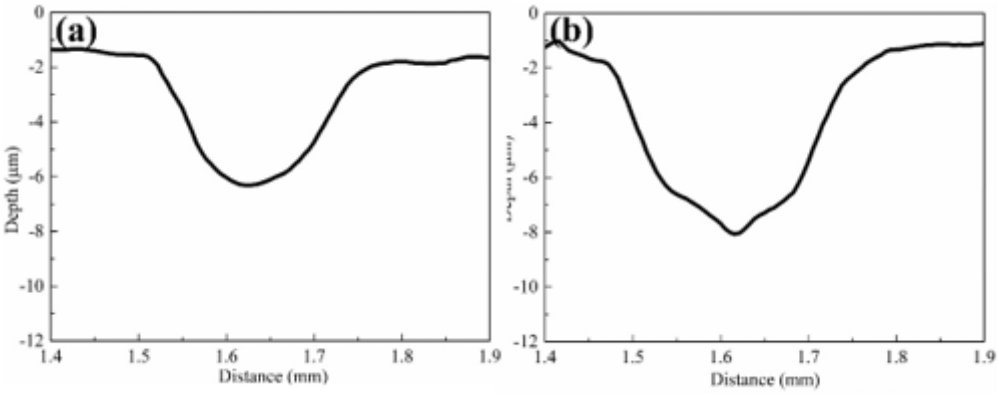

Figure 8

The two-dimension profile of the wear tracks of CBH (a) and CBN (b) composites at 800 °C.

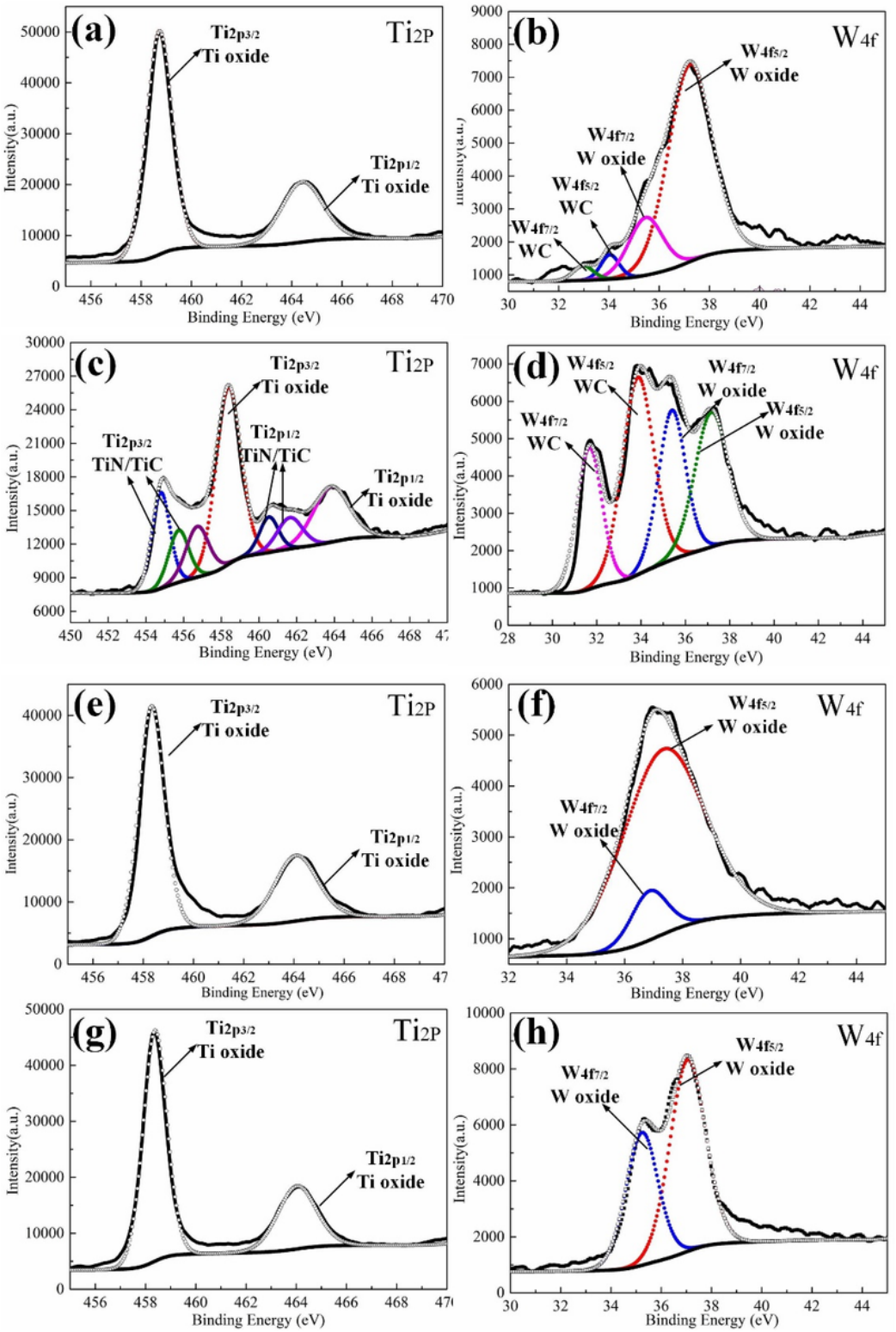

Figure 9

XPS analysis of the wear surface (a), (b) and (e), (f): 600 ℃ CBH and CBN composites; (c), (d) and (g), (h): 800 ℃ CBH and CBN composites.